Chapter 8
Conclusions

8.1 Synthesis of pentacoordinated and hexacoordinated gallium compounds

New series of pentacoordinated gallium(III) compounds bearing two equivalent of 2-methyl-8-hydroxyquinoline (HQ′) and one equivalent of a monodentate ligand were synthesised adapting the method proposed by Saphochak *et al.*[1,2]
The pentacoordination was achieved exploiting the strong chemical reactivity of phenol (HL^n) and carboxylic acid (HL'^n) derivatives towards gallium(III) metal cations to obtain complexes with the general formula $\mathbf{Q'_2GaL^n}$ and $\mathbf{Q'_2GaL'^n}$ respectively. Then mono-, bi- and polydentate ligands of these classes of compounds were adopted to study which possible functionalities can arise from their chemical structure in order to tune both chemical and physical properties of gallium complexes. With the same purpose, N,N bidentate ligands were chosen to synthesis new hexacoordinated gallium compounds with the general formula **[Q′$_2$Ga(N,N)][X]**. All synthesised materials were often obtained in good reaction yields.

8.2 Gallium complexes synthesised with phenol derivatives

In the series of $\mathbf{Q'_2GaL^n}$ compounds the pentacoordination is achieved with monodentate phenol derivatives as illustrated in **Figure 8.1**.

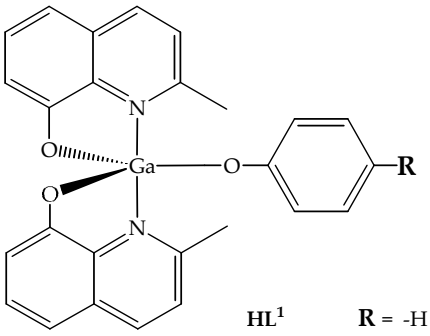

Q'_2GaL^n

HL^1 **R** = -H

HL^2 -CN

HL^3 $-NO_2$

HQ' = 2-methyl-8-hydroxyquinoline

Figure 8.1: *monometallic* Q'_2GaL_n *compounds.*

The good solubility in chloroform makes them good candidates for the solution-based methods in OLED fabrication techniques coupled with the absence of polymorphism depending on temperature, the high melting point may prevents film degradation due to the Joule effect generated by the electric current flow through the device.

8.2.1 Structural properties of Q'_2GaL^n

X-ray diffraction data were collected on single crystals obtained for slow diffusion of *n*-hexane in chloroform solution. The angles around the Ga(III) ion confirm a trigonal bipyramid geometry. The presence of a –CN and $–NO_2$ groups, in *p*-position, influence the crystallization of $Q'_2GaOC_6H_5$ compound in monoclinic space group while the $Q'_2GaOC_6H_4CN$ and $Q'_2GaOC_6H_4NO_2$ complexes crystallize in the triclinic being these complexes isostructurals. In all cases, both the Q′ ligands (named Q'_A and Q'_B) are involved in aromatic interactions with the symmetrical related rings; stacks with mixed chelates are not found. The Q'_A–Q'_A stacking is characterized by the same parameters in the

series of these gallium compounds, while the Q'_B–Q'_B aromatic interaction differs from complex **$Q'_2GaOC_6H_5$** to complexes **$Q'_2GaOC_6H_4CN$** and **$Q'_2GaOC_6H_4NO_2$**. HOMO–LUMO in metal quinolinates of the group XIII are localized on the quinolinate moieties and the charge transport capability depends on π–π stacking interactions.[3-7] Thus, the charge transport ability of **Q'_2GaL^n** series are taken in account considering the properties of their chemical structural focussing on which kind of influence could arise from the substituents on the phenolate ligands. Although the phenolate ligands are not involved in π–π stacking, they determine the supramolecular organization in the crystal packing as explained in the Paragraph 5.1.1.

The Q'_A and Q'_B stacking, between the pyridyl rings of **$Q'_2GaOC_6H_5$** compound show better overlap than that found for phenolate rings. In the supramolecular motif reported in **Figure 8.2**, can be evidenced the π–π stacking involving two neighbouring molecules generating extended two-dimensional chains.

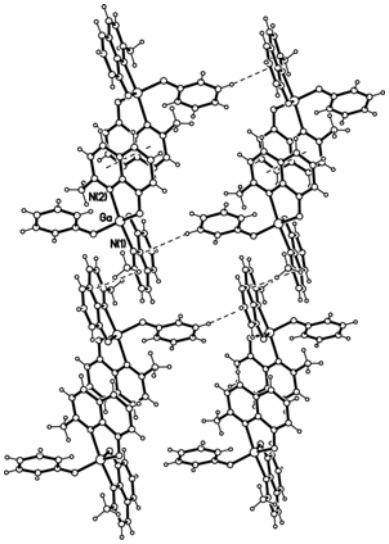

Figure 8.2: *supramolecular secondary motif of* ***$Q'_2GaOC_6H_5$*** *compound.*

Instead, crystal packings generated by **$Q'_2GaOC_6H_4CN$** and **$Q'_2GaOC_6H_4NO_2$** complexes are different. Each chelate exerts two contacts: a pyridyl–pyridyl stack, above the mean plane of the Q'_B ligand, and a phenolate–phenolate stack

below it involving three neighbouring molecules (**Figure 8.3**). In the case of the *p*-substituted phenol compounds the supramolecular motif displays a more extended π–π stacking than the one showed by **Q′$_2$GaOC$_6$H$_5$** compounds.

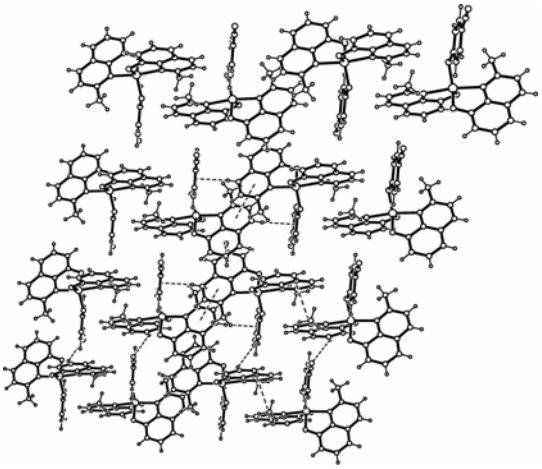

Figure 8.3: *supramolecular secondary motif of* ***Q′$_2$GaOC$_6$H$_4$CN*** *and* ***Q′$_2$GaOC$_6$H$_4$NO$_2$*** *complexes.*

8.2.2 Photophysical and electronic properties of ***Q′$_2$GaL^n*** *complexes*

Q′$_2$GaL^n complexes show similar absorption and emission profiles except for the **Q′$_2$GaOC$_6$H$_4$NO$_2$** compound in which is present an intense band at 304 nm, as can be observed in **Figure 8.4**.

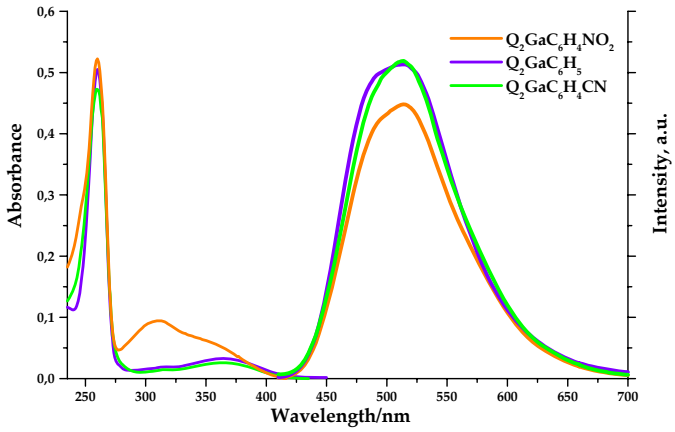

Figure 8.4: *absorption and emission spectra of* ***Q′$_2$GaOC$_6$H$_5$, Q′$_2$GaOC$_6$H$_4$CN, Q′$_2$GaOC$_6$H$_4$NO$_2$.***

All compounds are green emitters with good photoluminescence quantum yield (Φ_{PL}). These results are independent from the excitation wavelength except for Φ_{PL} of **Q′$_2$GaOC$_6$H$_4$NO$_2$** solution which is strongly reduced to 5% by changing the excitation wavelength at 304 nm. These results were compared with the calculated electronic states, illustrated in **Figure 8.5**, representing the relevant Kohn-Sham orbital energy levels. The study reveals that the HOMO is localized on the phenolate ligand (p_2) in **Q′$_2$GaOC$_6$H$_5$** compound, while the LUMO is localized on the Q′ ligands (q_2). This characteristic is not retained in the case of the other complexes, where the HOMO became localized on the Q′ chelant (q_1). The presence of the electron withdrawing groups –CN and –NO$_2$ produce the energy stabilization of the *p* orbital.

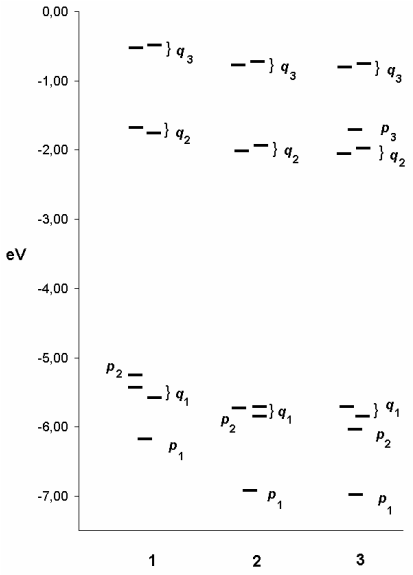

Figure 8.5: *Energy level scheme of relevant Kohn-Sham orbitals of complexes of* ***Q′$_2$GaOC$_6$H$_5$ (1), Q′$_2$GaOC$_6$H$_4$CN(2), and Q′$_2$GaOC$_6$H$_4$NO$_2$ (3).***

The photophysical behaviour matches the theoretical calculations. The absorption computed at 304 nm is associated to an electronic transition from the p$_2$ quinolinate-localized orbital to the p$_3$ orbital localized on the -NO$_2$ group (not reported in the case of **Q′$_2$GaOC$_6$H$_5$** and **Q′$_2$GaOC$_6$H$_4$CN** compounds).

This orbital is a π orbital with antibonding character localized between the oxygen and nitrogen atoms of the -NO_2 group. The electronic states can be classified in two classes: q-localized and p→q charge transfer. The low Φ_{PL} values collected for **Q′$_2$GaOC$_6$H$_4$NO$_2$** compound, measured exciting the complex on the band corresponding to the $p_2 \rightarrow p_3$ (304 nm) or to the $q_1 \rightarrow q_2$ (365 nm) transitions, are due to the low population of the emissive states. The computed HOMO-LUMO electronic state energies of **Q′$_2$GaL^n** are reported in **Table 8.1**.

Q′$_2$GaOC$_6$H$_5$		*Q′$_2$GaOC$_6$H$_4$CN*		*Q′$_2$GaOC$_6$H$_4$NO$_2$*	
p_2 *(HOMO)*	-5.20 *eV*	q_1 *(HOMO)*	-5.70 *eV*	q_1 *(HOMO)*	-5.73 *eV*
q_2 *(LUMO)*	-1.77 *eV*	q_2 *(LUMO)*	-2.02 *eV*	q_2 *(LUMO)*	-2.05 *eV*

Table 8.1: *HOMO – LUMO energy levels of* ***Q′$_2$GaL^n****.*

Absolute photoluminescence efficiency of **Q′$_2$GaL^n** complexes collected on film shows the same trend observed previously in solution. The measurements were registered with an integrating sphere (**Figure 8.6**) coupled with an He – Cd LASER as excitation source at excitation wavelength of 325 nm. The data were calculated following the method proposed by Greenam *et al.*.[8]

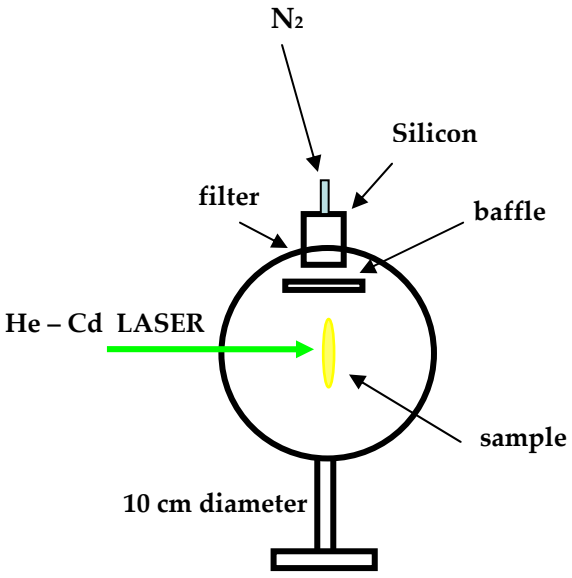

Figure 8.6: *integrating sphere.*

The collected data display a general decrease of the Φ_{PL} values; noteworthy, the **Q′$_2$GaOC$_6$H$_4$NO$_2$** compound shows almost a total quenching with a Φ_{PL} value of 1.8%. Luminescent materials are often doped with low concentration of other chemical species to enhance the electroluminescence and/or colour tuning.[9] Film mixtures of **Q′$_2$GaL^n**:TPD or **Q′$_2$GaL^n**:TPBI, in 10% and 20% in weight of the organic aromatic compounds, were characterised. **Table 8.2** is a qualitative representation of the obtained results.

Q′$_2$GaL^n	**:TPD** *Hole Transporting material*	**:TPBI** *Electron Transporting material*
Q′$_2$GaOC$_6$H$_5$	**red shift 507 → 520 nm** *strong enhancement*	**507 nm** *weak quenching*
Q′$_2$GaOC$_6$H$_4$CN	**red shift 507 → 520 nm** *strong quenching*	**500 nm** *strong enhancement*
Q′$_2$GaOC$_6$H$_4$NO$_2$	**red shift 507 → 520 nm** *weak quenching*	**507 nm** *strong enhancement*

Table 8.2: *blended film emission.*

These measurements may confirm the charge transport ability of the synthesised materials. As reported in the **Table 8.2** the supposed better hole transport materials, as **Q′$_2$GaOC$_6$H$_4$CN** and **Q′$_2$GaOC$_6$H$_4$NO$_2$**, show emission intensity enhancement when blended with an electro transport material. In that case, the **Q′$_2$GaOC$_6$H$_4$NO$_2$** compound performs better. This results are probably due to an efficient annihilation mechanism involving the **Q′$_2$GaOC$_6$H$_4$CN**$^{+\cdot}$ and **Q′$_2$GaOC$_6$H$_4$NO$_2$**$^{+\cdot}$ radical cations and the TPBI$^{-\cdot}$ radical anions to obtain **Q′$_2$GaOC$_6$H$_4$CN*** and **Q′$_2$GaOC$_6$H$_4$NO$_2$*** emissive species. While **Q′$_2$GaOC$_6$H$_5$** behaves as a poor hole transport material, because of a more efficient mechanism it seems to be an annihilation between **Q′$_2$GaOC$_6$H$_5$**$^{-\cdot}$

radical anion and $TPD^{+\cdot}$ radical cation to obtain the emissive species **$Q'_2GaOC_6H_5$***.

8.2.3 Application of Q'_2GaL^n in single layer device structure

Q'_2GaL^n compounds were taken in account to fabricate single layer device structures in the light of the results of their complete characterization. The synthesised materials were applied as electroluminescent layer obtained by spin-coating techniques from dichloromethane solutions. The architecture of the fabricated devices is illustrated in **Figure 8.7**; the emitting area was 4x1.2 mm^2.

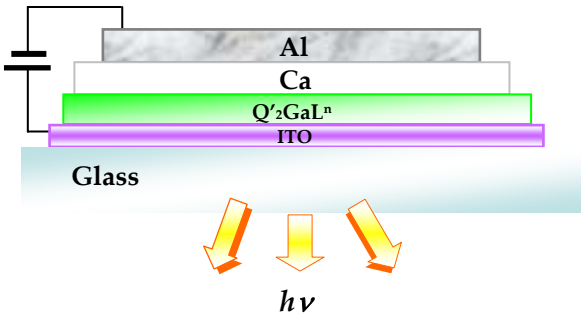

ITO/Q'_2GaL^n (70 nm)/Ca (20 nm)/Al (100 nm)

Figure 8.7: *single layer device architecture.*

When a bias voltage is applied to the electrodes the devices switch on illuminating the vacuum chamber with green light. Electroluminescence spectra were recorded for all device samples except for those obtained with **$Q'_2GaOC_6H_4NO_2$** (**3**) compound, as reported in **Figure 8.8**. The maximum emission values are red shifted of about 20 nm respect to the emission on film for **$Q'_2GaOC_6H_5$** (**1**) and **$Q'_2GaOC_6H_4CN$** (**2**) device samples, and of 30 nm for the **GaQ'_3** (**R**) sample due to the Frank-Condon relaxation.

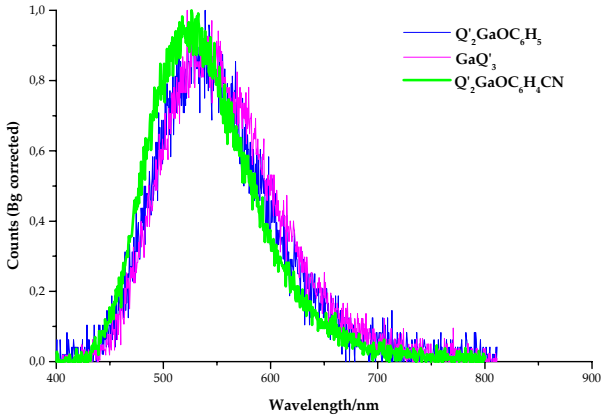

Figure 8.8: *electroluminescent spectra.*

There is not much difference in the computed LUMO energies between **Q'$_2$GaOC$_6$H$_4$CN** and **Q'$_2$GaOC$_6$H$_4$NO$_2$** compounds, while the LUMO energy value of **Q'$_2$GaOC$_6$H$_5$** is lower. Thus, the electron injection barriers between the emissive layer in sample **2** and **3** and the cathode, were almost the same. However, the device sample **2**, with **Q'$_2$GaOC$_6$H$_4$CN** as emissive layer, shows better *I-V* characteristics (**Figure 8.9**) and lower turn-on voltage (about 7 V), the same of the reference device **R**.

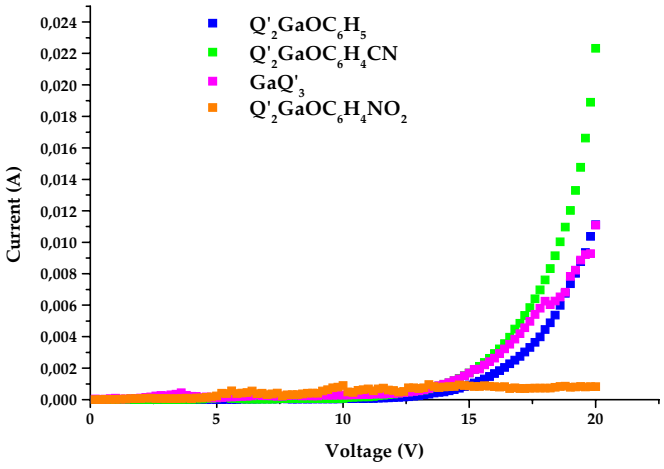

Figure 8.9: *I-V graphs.*

Current Density (464 mA/cm^2) and Luminance (465 Cd/m^2) were the highest values obtained ranging from 15 V to 20 V. This trend was confirmed by the Power Efficiency values, ten times higher than those exhibited by sample **3**, made with **$Q'_2GaOC_6H_5$** compound as electroluminescent layer.

The better External Quantum Efficiency (EQE%) at low voltages was registered for sample **2**, as reported in **Table 8.3**.

Q'_2GaL^n	*Power Efficiency lm/W (15 V)*	*Power Efficiency Cd/A (15 V)*	*External Quantum Efficiency %*
GaQ'_3 (R)	**4 10^{-3}**	**1.9 10^{-2}**	**0.1 % (17 V)**
$Q'_2GaOC_6H_5$ (1)	**3.4 10^{-4}**	**1.8 10^{-3}**	**0.044% (15 V)**
$Q'_2GaOC_6H_4CN$ (2)	**4 10^{-3}**	**1.8 10^{-2}**	**0.07% (14 V)**
$Q'_2GaOC_6H_4NO_2$ (3)	/	/	/

Table 8.3: *Power Efficiencies and EQE% device values.*

Figure 8.10: illustrate the recorded EQE% graph.

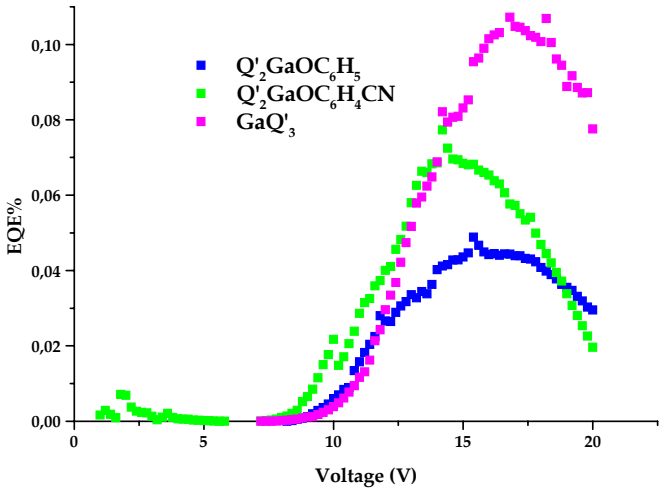

Figure 8.10: *External Quantum Efficiency (EQE%) graphs.*

Regarding the collected data, it seems that the better charge transport properties are exhibited by the sample **2**, fabricated with **Q'$_2$GaOC$_6$H$_4$CN** as electroluminescent layer. This is may be probably due to not only by the electrons but also by the better hole conduction, as predicted by crystallographic analysis, by computed electronic state and by the experimental photophysical characterization of the blended films.

Indeed the HOMO, mostly localized on the phenoxyde ring, is responsible of the hole conduction while the LUMO, mostly localized on the pyridyl ring, is responsible of electron conduction. The hole transport capability is not favoured for the **Q'$_2$GaOC$_6$H$_5$** compound. The hole transport properties should be improved for **Q'$_2$GaOC$_6$H$_4$CN** and **Q'$_2$GaOC$_6$H$_4$NO$_2$** by the phenolate-phenolate stack observed in crystal packing, although limited to a couple of adjacent molecules. Thus, an efficient charge recombination within the electroluminescent layer can be obtained.

These data may explain why sample **1**, fabricated with **Q'$_2$GaOC$_6$H$_5$** as electroluminescent layer, in spite of its electronic state energy compatible with the fabricated architecture, is less efficient electroluminescent material. While sample **3**, fabricated with **Q'$_2$GaOC$_6$H$_4$NO$_2$** as electroluminescent layer, shows the higher turn-on voltage. This sample shows light emission as reported in Photodiode Voltage graphs in Chapter 7, but not enough intense to be detected by the photodiode. Furthermore, the presence of a strong electron-withdrawing substituent could generate trap densities hampering the charge transport and recombination.

The better CIE coordinates in the PAL system, reported on the CIE diagram in **Figure 8.11**, are related to the **Q'$_2$GaOC$_6$H$_4$CN** device sample which shows better device performance than the reference sample fabricated with GaQ'$_3$.

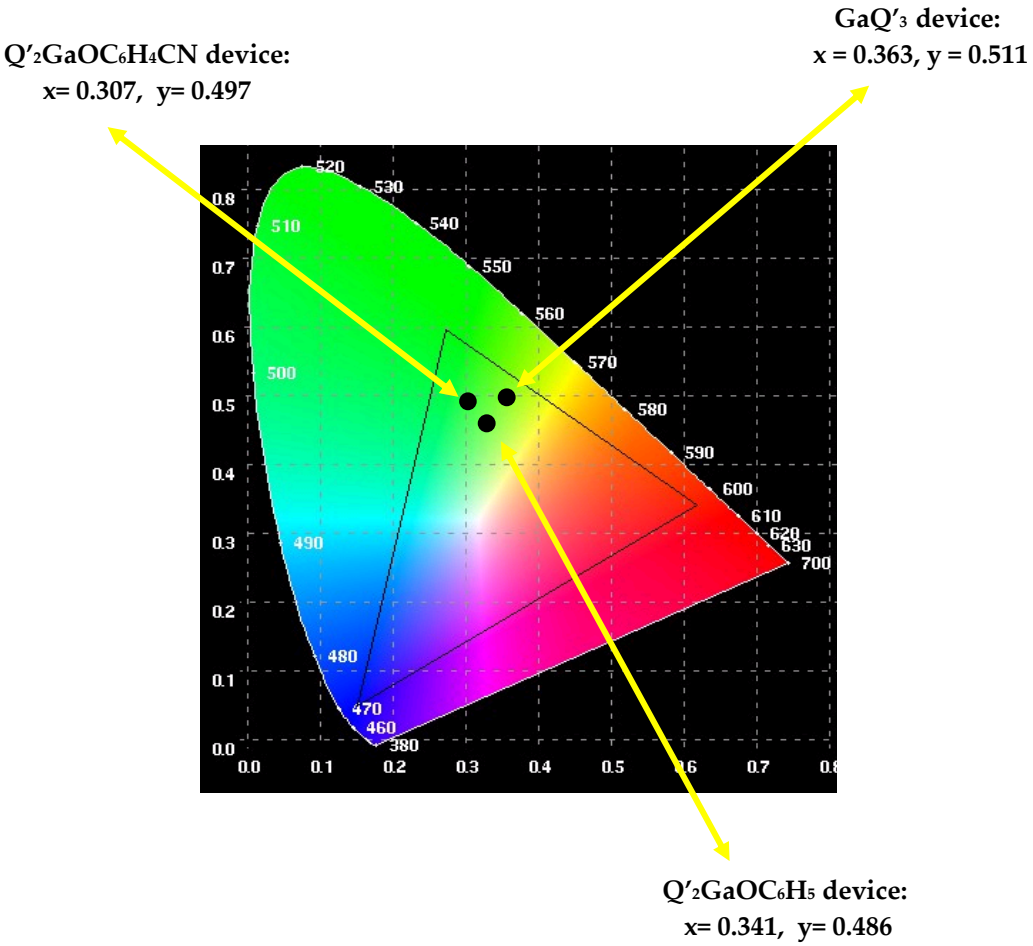

Figure 8.11: *CIE (x,y) chromaticity diagram.*

8.3 Gallium complexes synthesised with carboxylic acids derivatives

The synthesis of **Q′$_2$GaL′^{n}** series was performed choosing *p*-substituted benzoic acids derivatives as monodentate ligands. The obtained complexes are illustrated in **Figure 8.12**.

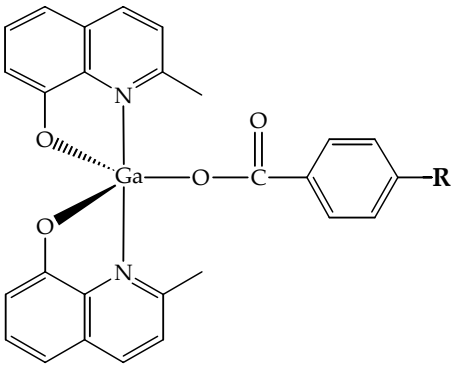

Q'$_2$GaL'$_n$

HL'^{n} = *p*-nitrobenzoic acid — **R =** -NO_2 — **Q'$_2$GaOOCC$_6$H$_4$NO$_2$**

p-hexyloxybenzoic acid — -$O(CH_2)_5CH_3$ — **Q'$_2$GaOOCC$_6$H$_4$O(CH$_2$)$_5$CH$_3$**

p-octiloxybenzoic acid — -$O(CH_2)_7CH_3$ — **Q'$_2$GaOOCC$_6$H$_4$O(CH$_2$)$_7$CH$_3$**

HQ'= 2-methyl-8-hydroxyquinoline

Figure 8.12: *pentacoordinated* ***Q′$_2$GaL′^{n}*** *compounds.*

Q′$_2$GaOOCC$_6$H$_4$O(CH$_2$)$_5$CH$_3$ was synthesised by substitution reaction of the phenoxyde ligand in the coordination sphere of **Q′$_2$GaOC$_4$H$_5$** compound with *p*-octyloxybenzoate, demonstrating the strong chemical affinity between gallium(III) and carboxylates. All complexes show good solubility in chloroform. The presence of an aliphatic chain in the molecular structure influences the melting point decrease. The characterization by X-ray diffraction analysis on single crystal reveals intermolecular π–π stacking interactions between quinolinate pyridinic rings of two adjacent molecules. On the base of the previous discussions, the pyridyl-pyridyl stack feature suggests an electron

transport capability of this material. Furthermore, the compounds bearing the $-NO_2$ group on the monodentate ligand shows low photoluminescence quantum yield about 8%, while the compounds bearing the aliphatic chains in the molecular structure exhibit high photoluminescence quantum.

8.4 Perspective studies

The studies illustrated previously suggest a better exploitation of the luminescent properties of the *Q′₂Ga-* fragment. The pentacoordination enhance chemical and morphological stability and good photoluminescent properties[1] coupled with interesting charge transport features arising from the crystalline organization observed for **Q′₂GaLⁿ** and **Q′₂GaL′ⁿ** compounds.

The studies on bibentate or polydentate ligands were conducted to obtain more chromophores in the same structure. In order to study if such a system can act as an antenna system to exploit energy transfer mechanism between a donor and an acceptor in the same molecular structure avoiding the degradation of blended system due to phase separation. **ZnTPP(OGaQ′₂)₄** heterobimetallic compound was a prototype of this idea.[10,11]

The high chemical reactivity between gallium(III) and carboxylates was taken in account to synthesis a new series of compounds in which the pentacoordination is achieved with trisubstituted benzoic acids.

The strong affinity between quinoline and gallium cation is competitive with the formation of other chemical species so that hexacoodinated quinolinate gallium compounds reported in litterature are the neutral homoleptic complexes as GaQ_3 or GaQ'_3.[6] This unfavourable chemical behaviour was avoided, hence hexacoordinated heteroleptic quinolinate compounds were

investigated. This was done to introduce a further functionalization, keeping at the same time the luminescent properties of *Q'₂Ga-* fragment. Although the studies mentioned are in the early stage, and further analysis are under investigation, some suggestions could arise to the future perspective applications of this kind of multifunctional material.

8.4.1 Polymetallic gallium compounds

The possibility to obtain bimetallic compound with biphenols and bicarboxylic acids suggested to synthesis polymetallic compounds using porphyrin derivatives bearing phenols and carboxylic acids in *meso* positions. For that reason **H₂TPP(OH)₄** and **H₂TPP(COOH)₄** porphyrins were chosen as rigid extended heteroaromatic macrocycle. Four *Q'₂Ga-* fragments in peripheral position and a metal cation as zinc in the porphyrinic core were introduced in the same structure (**Figure 8.13**).

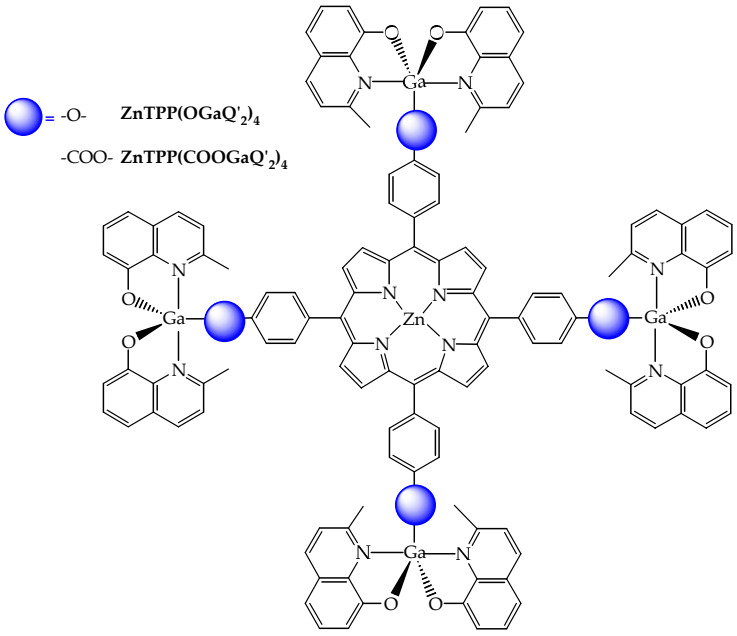

Figure 8.13: *polymetallic* ***ZnTPP(OGaQ'₂)₄*** *and* ***ZnTPP(COOGaQ'₂)₄*** *compounds.*

The synthesised **ZnTPP(OGaQ′$_2$)$_4$** and **ZnTPP(COOGaQ′$_2$)$_4$** compounds show differences in aspect and solubility: **ZnTPP(COOGaQ′$_2$)$_4$** is a brown insoluble powder while **ZnTPP(OGaQ′$_2$)$_4$**, a dark blue solid, is soluble in methanol allowing further characterisations.

8.4.1.1 Photophysical properties of polymetallic compounds

The synthesised heterobimetallic compounds illustrated exhibit in the absorption and emission spectra the contribution of both *Q′$_2$Ga*– lateral pendant and metallated porphyrinic core. The only substantial difference between **ZnTPP(OGaQ′$_2$)$_4$** and **ZnTPP(COOGaQ′$_2$)$_4$** lies in the absorption spectra. **ZnTPP(COOGaQ′$_2$)$_4$** displays four Q bands in spite of the introduction of zinc in the carboxylate porphyrinic core. Although **ZnTPP(OGaQ′$_2$)$_4$** is a mixture of product this does not affect the photophysical observation. **Figure 8.14** illustrate the emission spectra of **ZnTPP(OGaQ′$_2$)$_4$** exciting the *Q′$_2$Ga*– fragment at at 256 nm or the Zn-porphyrinic core at 424 nm.

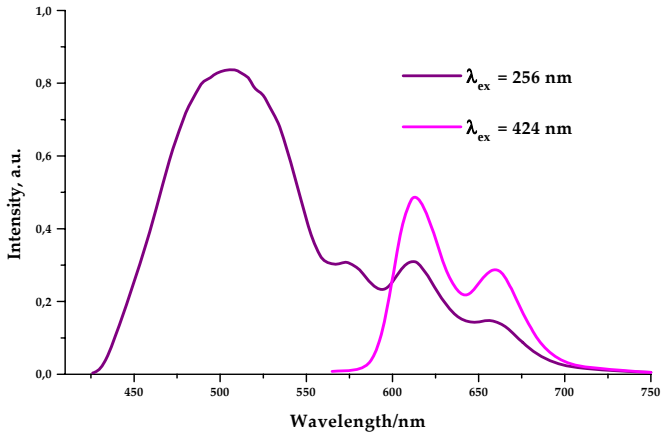

Figure 8.14: *double emission at different excitation wavelengths.*

The possibility to exploit a charge transfer mechanism from the *Q′$_2$Ga*– lateral pendant as donor group (D) to the Zn-porphyrinic core as acceptor group (A) is

hampered by tilted conformation the phenol rings, with respect to the porphyrin ring preventing a Dexter energy transfer mechanism. Further the lifetime τ_D and τ_{DA} prevent a favourable κ^2 factor. However, two different chromophores are linked in the same structure. By choosing a suitable excitation wavelength it is possible to switch between to different emissions wavelength, thus, between two different colours, obtaining a simple optical binary mechanism to communicate information.

8.4.2 Gallium complexes synthesised with trisubstituted carboxylic acids derivatives

Q'$_2$GaL'^{n} showed in **Figure 8.15**, were synthesised adapting the synthetic protocol described in Chapter 5. The monodentate ligands, HL'^{n}, were synthesised following a procedure reported in literature.[12,13]

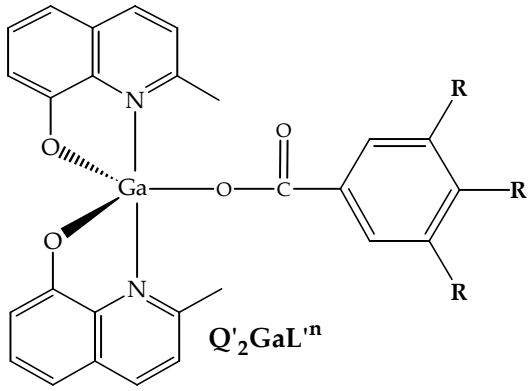

HL'^{4} = $HOOCC_6H_2(OC_6H_{13})_3$ **R=** $-OC_6H_{13}$

HL'^{5} = $HOOCC_6H_2(OC_{14}H_{29})_3$ $-OC_{14}H_{29}$

HQ' = 2-methyl-8-hydroxyquinoline

Figure 8.15: Q'$_2$GaL'^{n} compounds.

Then, **Q'$_2$GaOOCC$_6$H$_2$(OC$_6$H$_{13}$)$_3$** and **Q'$_2$GaOOCC$_6$H$_2$(OC$_{14}$H$_{29}$)$_3$** were obtained. The reaction yields were quite low because of the steric hindrance of the three aliphatic chains. These complexes show solubility also in ethers and slightly in alcohols. This aspect is an important feature to improve the OLED fabrication

techniques. As expected, the presence of long aliphatic chains in **Q′$_2$GaOOCC$_6$H$_2$(OC$_{14}$H$_{29}$)$_3$** induce mesomorphysme as evidenced by DSC analysis. X-ray diffraction data collected on single crystal (**Figure 8.16**), confirm the trigonal bipyramid geometry. Further analysis are still under investigation.

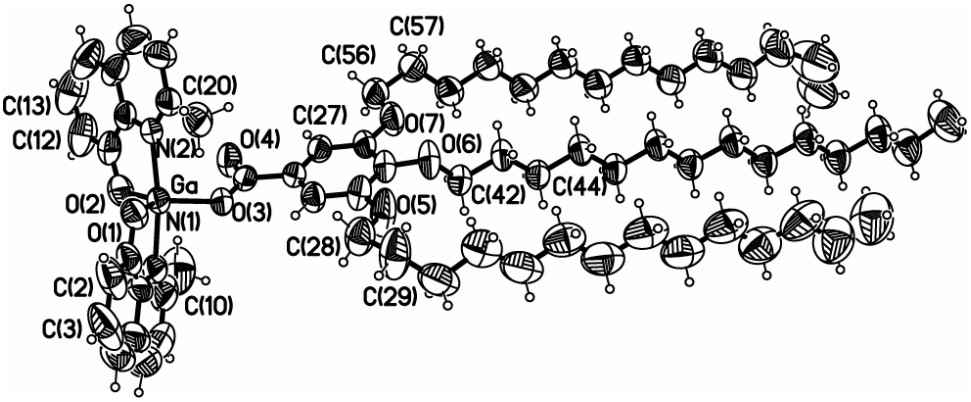

Figure 8.16: *Perspective view of* ***Q′$_2$GaOOCC$_6$H$_2$(OC$_6$H$_{13}$)$_3$*** *complexes with atomic numbering scheme (ellipsoids at the 50% level).*

8.4.2.1 Photophysical properties of ***Q′$_2$GaL′^{n}*** *complexes*

The absorption and emission spectra profile of this series of **Q′$_2$GaL′^{n}** complexes are similar and typical of quinolinate gallium compound as illustrated in **Figure 8.17**.

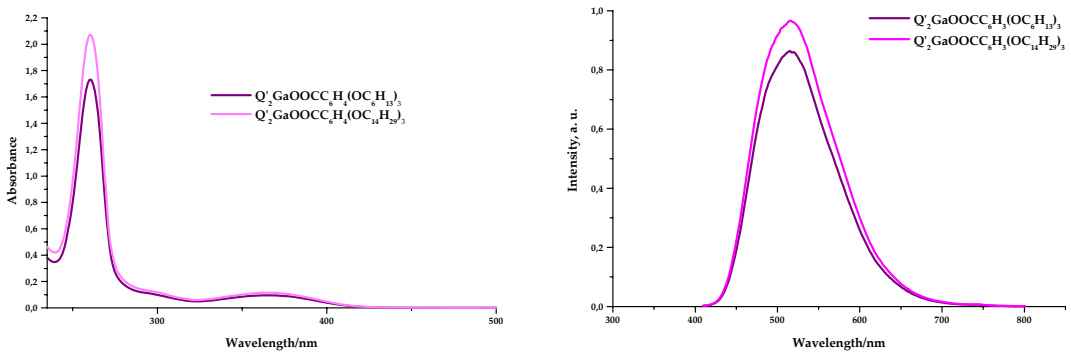

Figure 8.17: *absorption and emission spectra of* ***Q′$_2$GaL′^{n}*** *.*

Compounds bearing aliphatic chains show high photoluminescent quantum yield in dichlorometane solution and strong emission intensity on film. The enhancement of the Φ_{PL} value may arise from a possible self organization of the molecules due to the aliphatic tails. Further investigation could explain if the collected data may arise from anisotropic mechanical and optical properties induced by the supramolecular organization. Furthermore, the ordered oriented systems can generate polarised emission. It is possible to control the morphological stability of the materials and to avoid phase separation.[12,13]

8.4.3 First consideration on ionic hexacoordinated gallium compounds

New ionic hexacoordinated gallium complexes with the general formula **[Q'$_2$Ga(N,N)][X]**, (N,N= 2,2'bipyridine, 1,10-phenanthroline) (X= NO_3^-, PF_6^-) (**Figure 8.18**) were synthesised. Noteworthy, charged bis-quinaldinate gallium(III) compounds are unknown in literature.

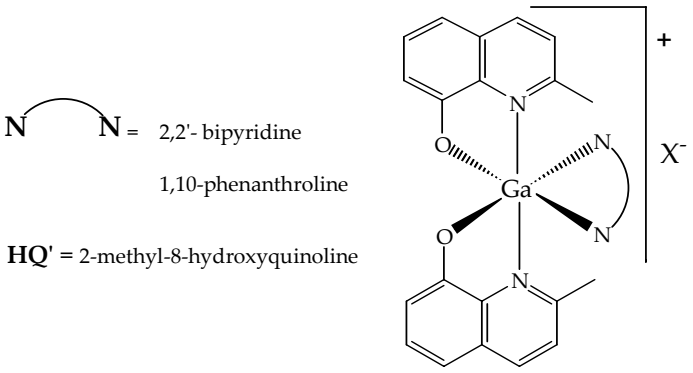

Figure 8.18: *hexacoordinated* ***[Q'$_2$Ga(N,N)][X]****, (X= NO_3^-, PF_6^-) compounds.*

All complexes show solubility in dichoromethane, DMSO and acetone. Some chemical instability could arise in coordinating solvents, as evidenced in the ^{1}H NMR spectra collected in DMSO and $CDCl_3$ for **[Q'$_2$Ga(phen)][X]** complexes. Furthermore, in the case of a technological application, these compounds could

be sensible to ambient moisture as typically showed by the quinolinate metal complexes. X-ray diffraction on single crystal confirm that the hexacoordination approximates an octahedral geometry (**Figure 8.19**).

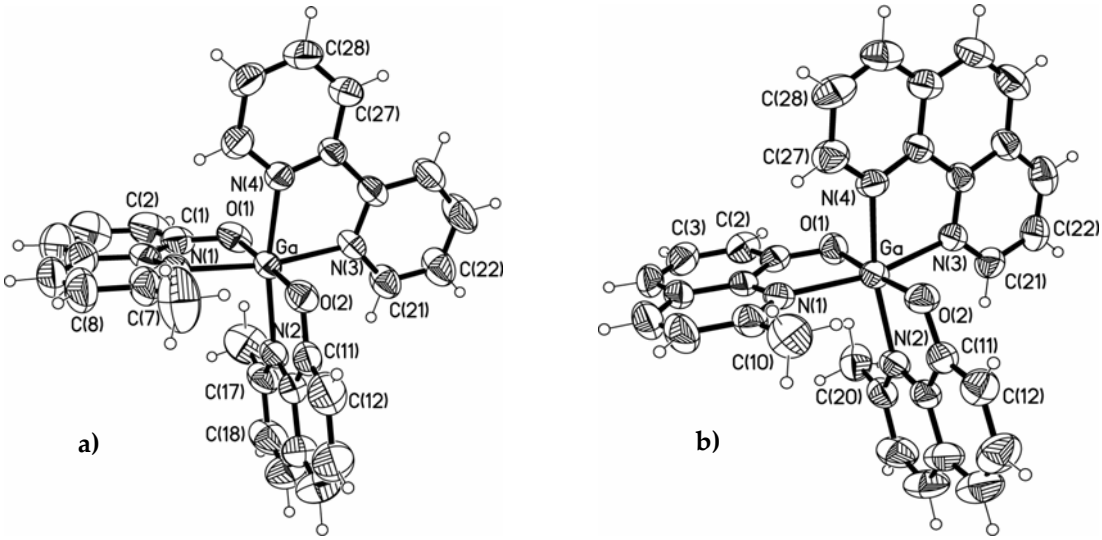

Figure 8.19: *Perspective view of the complexes of* ***a)*** ***[Q'$_2$Ga(bipy)][X]*** *and* ***b)*** ***[Q'$_2$Ga(phen)][X]*** *cations with atomic numbering scheme (ellipsoids at the 50% level).*

8.4.4 Photophysical and cyclovoltammetric properties

The absorption and the emission spectra are the characteristic spectral profile of the bisquinaldinate gallium compounds. **[Q'$_2$Ga(N,N)][NO$_3$]** compounds exhibit good Φ_{PL} values, ranging from 15% to 25%. The Φ_{PL} values related to the **[Q'$_2$Ga(N,N)][PF$_6$]** compounds are strongly reduced. It seems, at first observation, that this quenching may concern the presence of PF_6 as counter ion. Further investigations are required to properly comment this behaviour. It is useful to remark that these complexes are test compounds: the luminescent properties may be tuned and enhanced introducing different substituents on the aromatic ligands and/or changing the nature of the counter ions.

The photophysical results linked with the CV data suggest that the HOMO energy in **[Q′$_2$Ga(N,N)][X]** is probably distributed on the quinolate fragments. The calculated values are comparable with those calculated for pentacoordinated gallium phenolate compounds.[5] The HOMO levels are localised on the *Q′$_2$Ga-* fragment as expected for this class of gallium compounds, while LUMO energy levels estimated by CV are higher than those calculated for the cited pentacoordinated gallium complexes. This observation could suggest that the LUMO energy distribution should be more localised on the N,N chelating ligands. This could explain the different reversibility observed on the voltammograms for the reduction processes of the two complexes. The data are reported in **Table 8.4**.

[Q′$_2$Ga(N,N)][PF$_6$]	*E^{ox} (V) vs. Fc^+/Fc*	*E^{red} (V) vs. Fc^+/Fc*	*HOMO (eV)*	*LUMO (eV)*	*Band Gap (eV)*
[Q′$_2$Ga(bipy)][PF$_6$]	+ 0,94 (Irr.)	- 1,60 (Rev.)	- 5,74[b]	- 3,2[b]	2,54
[Q′$_2$Ga(phen)][PF$_6$]	+ 0,94 (Irr.)	-1,66 (Irr.)	- 5,74[b]	- 3,14[b]	2,6

Table 8.4: *cyclic voltammetric data of* ***[Q′$_2$Ga(N,N)][PF$_6$]****.*

The **[Q′$_2$Ga(N,N)][X]** displayed luminescence and interesting redox features that deserve to be tested in solid-state light-emitting devices based on small-molecules.[14]

The functioning of this kind of devices is due to an electrochemical mechanism, associated to the relatively slow redistribution of the counter ion within the device. In the present study the ionic molecular species present two kind of counter ions differing each other in the molecular dimension. This factor may influence the ionic transport mechanism through a layered material as thin solid film.

8.5 Conclusive remarks

The experimental work give rise luminescent materials coupled with other functionalities as charge transport properties. A further target was to enhance morphological stabilities of the synthesised materials in the solid state. The syntheses were carried out in aqueous solution or alcohol, under mild conditions. This is an important aspect for the design of environment friendly synthetic protocols. The reactivity of gallium towards monodentate or bi- or polydentate ligands was explored to tune the chemical and physical properties related to the Q'_2Ga- chromophore.

Concerning the monometallic $\mathbf{Q'_2GaL^n}$ compounds obtained with phenol derivatives, a complete pathway was followed, starting from molecular design throughout the characterization, towards the verification of the supposed features with the fabrication of OLED structures. All the supposed charge transport properties derived from the analysis of the collected data were confirmed. Changes in the molecular chemical structure determine the properties of the bulk material. The evidence in the case of $\mathbf{Q'_2GaL'^n}$ compounds, is the enhanced photoluminescence, probably due to the organization controlled by the aliphatic chain. These may be considered as flexible spacers between the chromophores in a covalent host-guest system. The aliphatic chains act as a host material covalently linked with a guest, in that case the coordinated metal. Another point of view may be to have a polar "head" (Q'_2Ga- fragment) and an apolar "body" (the aliphatic tails) in the same structure. Thus, the order of these materials in the solid state and the properties may be controlled to induce anisotropic properties in the bulk. As first observation in the case of the synthesised materials the enhancement of photoluminescence quantum yield.

Heteropolymetallic compounds are test compounds synthesized to realize a structure promoting energy transfer mechanism between different chromophores as host-guest dyes covalently linked together in the same chemical structure. The challenge is to avoid the blended systems applied in device fabrication, that often show morphological instability. For this purpose the chemical structure may be modulated, changing the metals in the porphyrinic core, or choosing a different heteroaromatic macrocycle to enhance optical properties or promote oriented functionalities avoiding morphological degradation.

A further synthetic route has produced new heteroleptic hexacoordinated ionic gallium complexes. These compounds are green emitters bearing ionic structure. The possibility to exploit these features as coupled properties is the challenge of further studies. Ionic structure could improve the device performance because of the ionic conductivity in the bulk of the emissive layer. As experimented in solid state electroluminescent devices, the ionic conductivity depends on the counter ion mobility and also on the type of the counter ions. This is an important feature in order to control the charge injection. Since ions are integral part of this materials, ionic conductivity can occur without phase separation as in the light-emitting electrochemical cells fabricated by dispersing salts into organic semiconductors. A further development may take in account other kind of counter ions or N,N bidentate ligand.

REFERENCES

1. Sapochak, L. S.; Burrows, P. E.; D. Garbuzov, D. M. Ho, S. R. Forrest, M. E. Thompson, *J. Phys. Chem.* **1996**, *100*, 17766.

2. Schmidbaur, H.; Lettenbauer, J.; Wilkinson, D. L.; Muller, G.; Kumberger, O. *Z. Naturforsh.* **1991**, *46b*, 901.

3. Burrows, P. E.; Shen, Z.; Bulovic, V.; McCarty, D. M.; Forrest, S. R.; Cronin, J. A.; Thompson, M. E. *J. Appl. Phys.* **1996**, *79*, 10, 7991.

4. Burrows, P. E.; Forrest, S. R. *Appl. Phys. Lett.* **1994**, *64*, 17, 2285.

5. Crispini, A.; Aiello, I.; La Deda, M.; De Franco, I.; Amati, M.; Lelj, F.; Ghedini, M. *Dalton Trans.* **2006**, 5124.

6. Brinkmann, M.; Fite, B.; Pratontep, S.; Chaumont, C. *Chem. Mater.* **2004**, *16*, 4627.

7. Wang, Y.; Zhang, W.; Li, Y.; Ye, L.; Yang, G. *Chem. Mater.* **1999**, *11*, 530.

8. Greenham, N. C.; Samuel, I. D. W. et al., *Chem. Phys. Lett.* **1995**, *89*, 241.

9. Anderson, J. D.; McDonald, E. M.; Lee, P. A.; Anderson, M. L.; Ritchie, E. L.; Hall, H. K.; Hopkins, T.; Mash, E. A.; Wamg, J.; Padias, A.; Thayumanavan, Barlow, S.; Marder, S. R.; Jabbour, G. E.; Shaeen, S.; Kippelen, B.; Peyghambarian, N.; Wightman, R. M.; Armstrong, N. R. *J. Am. Chem. Soc.* **1998**, *120*, 9646.

10. Kwong, C.R.; Sibley, S.; Dubovoy, T.; Baldo, M., Forrest, S. R.; Thompson, M. E. *Chem Mater.* **1999**, *11*, 3709.

11. Harriman, A.; Hissler, M.; Trompette, O.; Raymond, Z. *J. Am. Chem. Soc.* **1999**, *121*, 2516.

12. Binnemans, K.; Guillon D.; Lodewyckx, K.; Cardinaels, T.; Parac-Vogt, T.; Bourgogne, C.; Donnio, B. *Eur. J. Chem.* **2006**, 150.

13. Bondzic, S.; de Wit, J.; Polushkin, E.; Schouten, A. J.; ten Brinke, G.; Ruokolainen, J.; Ikkala, O.; Dolbnya, I.; Bras, W. *Macromolecules* **2004**, *37*, 9517.

14. Parker, S. T.; Slinker, J. D.; Lowry, M. S.; Cox, P. M.; Bernhard, S.; Malliaras, G. G. *Chem. Mater.* **2005**, *17*, 3187.